MODELLING OF DIRECT-STRIKE LIGHTNING COUPLING BY A TRANSFER FUNCTION TECHNIQUE

D. T. Auckland and R. F. Wallenberg
Syracuse Research Corporation, Syracuse, New York
J. A. Birken
Naval Air Systems Command, Washington, D. C.

ABSTRACT

A transfer function approach is applied to the problem of lightning coupling into internal aircraft avionic circuits. This approach allows a systematic procedure for determining transient levels induced on interior aircraft circuits due to exterior interference fields such as those caused by nearby or direct-strike lightning. Unique in the approach used here is the use of a triangular patch model for the exterior surface of the aircraft with all points of entry (POEs) closed. A moment method procedure is then used to find the ("short circuit") skin current in the frequency domain. This current interacts with all the POEs, described by either measured or theoretically calculated transfer functions, in a secondary interaction problem to create interior penetrating fields. These interior fields are used to derive distributed voltage and current sources which excite a transmission line model of a wire harness or cable bundle. Further levels of coupling are indicated along with their concomitant transfer functions.

INTRODUCTION

THE GENERAL PROBLEM of analytically determining the susceptibility of interior aircraft avionics circuitry to upset or damage caused by an external electromagnetic threat is inherently complicated. To facilitate the analysis, two principle assumptions concerning the electromagnetic coupling phenomenon are made at the outset:

- Linearity of material media
- Interaction level decoupling

The meaning of the first assumption is obvious and test results show that it is generally valid for bulk cable current responses. The second assumption means that the aircraft has no effect on the source, the interior compartments have no effect on the external skin currents, and the interior circuits have no effect on the interior fields. It is easy to construct pathological cases for which the second assumption is theoretically invalid. Measured results, however, indicate that for a great many cases, it is a reasonable assumption.

Figure 1 illustrates a matrix of possible interaction levels where, at each level, a source interacts with a characteristic to produce a result. Further simplifying assumptions concerning the threat, the external physical detail of the aircraft, and the interior detail of the circuit in question must still be made in order to make the problem tractable. Errors introduced at each characteristic model level combine to cast accumulative uncertainty at each successive result level. Hopefully, careful comparison between computations and measured results will aid in refining characteristic models and reducing result error.

Using the first two assumptions, and working in the frequency domain, one may express the results of level D in Fig.1 by the following equations:

$$\begin{Bmatrix} V_B(f) \\ I_B(f) \end{Bmatrix} = D(f)\, T_{AC}(f)\, T_{POE}(f) \begin{Bmatrix} T_C^V(f) \\ T_C^I(f) \end{Bmatrix} T_T(f)\, T_P(f) \qquad (1)$$

where:

- $V_B(f)$, $I_B(f)$ = Voltage and current transfer function at input of susceptible device (avionics box)
- $D(f)$ = Threat driving function spectrum
- $T_{AC}(f)$ = Band-limited approximation to impulse response of aircraft
- $T_{POE}(f)$ = Point-of-entry (POE) trans-transfer function
  - Z_{st} = Material shielding transfer impedance
  - Y_j = Joint admittance
- $T_C(f)$ = Transfer functions accounting for compartment detail T_C^V, T_C^I
- $T_T(f)$ = Transmission line coupling transfer function including cable shielding
- $T_P(f)$ = Avionics box protection function including penetration and circuit protection functions

This juxtaposition of transfer functions is illustrated pictorially in Fig. 2. Further detail concerning the above transfer function approach to electromagnetic coupling applied to aircraft is given in [1]* and [2]. Examples of some of the above characteristic transfer functions are illustrated pictorially in Fig. ..

DESCRIPTION OF THE METHOD

The double exponential time function

$$D(t) = A(e^{-\alpha t} - e^{-\beta t}) \qquad (2)$$

is often used to model lightning waveforms [3] where the parameters α and β may be adjusted to change the rise time $1/\beta$ and fall time $1/\alpha$ of the lightning return stroke. This simple double exponential model is assumed to sufficiently characterize the behavior of the current in

*Numbers in brackets indicate references at end of paper.

the lightning channel. In this model, the lightning attachment to the aircraft is well underway and the source of the channel is treated as a very high impedance current generator so that the aircraft has no loading effect on the channel.

When a conducting aircraft becomes part of the path of a lightning channel current, a large charge displacement takes place at certain "junction" points on the aircraft where the channel enters and exits. These points are deemed "entry" and "exit" points, where the conventional reference direction of current is implied to denote charge transfer. Here we assume that the entry and exit points are given and that they coincide with nodes in the triangular surface patch model [4, 5, and 6] of the aircraft skin. This will, in fact, be the case when modelling an experimental setup where current injection points are well defined [7]. Further details concerning the computation of direct strike skin currents may be found in [6] and details concerning direct strike test methods may be found in [8, 9, and 10] for operational aircraft.

A widely used and readily available data base which models aircraft skin by surface patches is the so-called NASTRAN data base [11]. An example of this is shown in Fig. 3 for the Black Hawk helicopter. In order to solve for the skin currents by the method of moments, a reduced data base consisting of triangular surface patches is created. Examples of these are shown in Figs. 4 through 7 for the Black Hawk helicopter and F-14 fighter aircraft. Here we have picked various direct-strike entry and exit points and pictorially represented the normalized 1 MHz component of the direct strike skin current density distribution. Vectors are drawn at the centroid of each visible triangular face to indicate the direction of $\mathrm{Re}\{\underline{J}_S\ e^{j\omega t}\}$ for a particular ωt, where the skin current phasor, $\underline{J}_S$, is found at each centroid from the coefficients of triangular patch expension at adjacent edges. For the pictures shown here, ωt was taken to be zero. Current magnitude information may be obtained from Fig. 5 and 7 where numbers from 0 to 9 are printed on each triangular face to indicate the magnitude of the current at that face scaled relative to the maximum current.

At level B of the interaction table the skin currents $\underline{J}_S$ and charges ρ_S, which are obtained from $\underline{J}_S$ by the equation of continuity, drive a model for the particular POE under consideration. This may be a composite avionics bay door, or a joint or seam in the aircraft skin. For each case, we relate internal sources $\underline{J}^{int}$, $\underline{M}^{int}$ to $\underline{J}_S$ by:

° Joints - joint admittance Y_j

$$\underline{M}^{int} = Y_j^{-1} \underline{J}_S \tag{3}$$

° Composite Panels - transfer impedance Z_t

$$\underline{M}^{int} = Z_t \underline{J}_S \tag{4}$$

$T_{POE}(f)$ is thus defined by Z_t or Y_j^{-1} depending on the POE under consideration. The effects of more than one POE are linearly superposed.

The interior sources radiate in the presence of an interior compartment to produce the interior fields $\underline{E}^{int}$ and $\underline{H}^{int}$. The transfer functions T_C^V and T_C^I account for the effect of the compartment detail. An example of the effects of the compartment transfer functions is shown in Fig. 8 where a two-dimensional field mapping of the F-14 cockpit is illustrated for a nose-tail strike.

At successive levels of interaction, the complexity of the problem can exponentially increase if one tries to accurately model the excitation of convoluted masses of cable bundles. Here we assume that a bundle of wires routed from one box to another within the penetrated compartment of interest may be modeled by a transmission line where a single TEM mode is assumed. The interior fields are used to determine distributed voltage and current excitations along the line so that we may write

$$\begin{Bmatrix} V_B(f) \\ I_B(f) \end{Bmatrix} = \int_{\ell=0}^{L} \begin{Bmatrix} G_B^{VI}(f,\ell)\, I_s(f,\ell) + G_B^{VV}(f,\ell)\, V_s(f,\ell) \\ G_B^{II}(f,\ell)\, I_s(f,\ell) + G_B^{IV}(f,\ell)\, V_s(f,\ell) \end{Bmatrix} d\ell \tag{5}$$

The functions G_B are obtained from a straightforward solution of the transmission line equations using impulsive voltage and current sources.

In some cases, the bulk voltages and currents may be used to define an avionics box protection function T_P given by

$$\begin{bmatrix} T_p^I \\ T_p^V \end{bmatrix} = \begin{bmatrix} I_B \\ V_B \end{bmatrix} - \begin{bmatrix} \hat{I}_B \\ \hat{V}_B \end{bmatrix} \quad (\mathrm{dB}) \tag{6}$$

where $\hat{I}_B$ and $\hat{V}_B$ are the threshold box current and voltage damage levels, respectively. T_p gives the additional box protection required against the computed bulk voltage V_B and current I_B.

CONCLUSION

The utility of the above procedure is made apparent when put in the form of a user-oriented design program. Data bases which describe the various frequency domain transfer functions are accessed as needed and can be updated or changed depending upon design constraints. Once the exact location of a cable bundle is described inside the aircraft, as well as all of its associated POEs, induced current and voltage levels may be computed for a given lightning stroke situation. An example of this type of computation for a "generic" cable harness in the nose wheel well of an F-14 aircraft is given in Fig. 9.

REFERENCES

1. R.F. Wallenberg, D T. Auckland, and J.A. Birken, "A Transfer Function Approach to Coupling to the Interior of a Composite/Metal Aircraft Based on a Triangular Patch Model", IEEE International Symposium on EMC, Santa Clara, eptember 1982.

2. R. Wallenberg, et. al., "Advanced Composite Aircraft Electromagnetic Design and Synthesis", Syracuse Research Corporation Interim Report SRC TR 79-490, Syracuse, New York, April 1980.

3. E.T. Pierce, et. al., "Natural Lightning Parameters and their Simulation in Laboratory Tests", SRI Project 3062, February 1976.

4. S.M. Rao, "Electromagnetic Scattering and Radiation of Arbitrarily Shaped Surfaces by Triangular Patch Modelling", Ph.D. Dissertation, University of Mississippi, August 1980.

5. S.M. Rao, D.R. Wilton, and A.W. Glisson, "Electromagnetic Scattering by Surfaces of Arbitrary Shape", IEEE Transactions on Antennas and Propagation, Vol. AP-30, May 1982, pp 409-418.

6. D.T. Auckland and C.C. Cha, "A Model for Direct-Strike Lightning Excitation of a Conducting Body", IEEE International Symposium on EMC, Santa Clara, CA, September 1982.

7. FLLASH (Full Level Lightning Aircraft System Hardening) Tests performed on the F-14 and F-18 aircraft at Albuquerque, NM, under the direction of J.A. Birken, Naval Air Systems Command, Spring-Summer 1982.

8. R.A. Perala, "Full Level Lightning Aircraft System Hardening (FLLASH) Test Plan for Lightning Testing of the F/A-18A", prepared for Syracuse Research Corporation under Purchase Order 6008 and Naval Air Systems Command Prime Contract N00019-82-C-0088, March 1982.

9. R.A. Perala, "Full Level Lightning Aircraft System Hardening (FLLASH) Test Plan for Lightning Testing of the F-14A Aircraft", prepared for Syracuse Research Corporation under Purchase Order 6008 and Naval Air Systems Command Prime Contract N00019-82-C-0088, February 1982.

10. J.D. Robb and J.D. Herring, "Lightning Tests Sikorsky Black Hawk", prepared by Lightning and Transients Research Institute, 2531 West Sumner Street, St. Paul, Minnesota, for Sikorsky Aircraft Company under Purchase Order 208578, January 1980.

11. H.G. Schaeffer, "MSC/NASTRAN Primer, Static and Normal Model Analysis", Schaeffer Analysis, Inc., 1979.

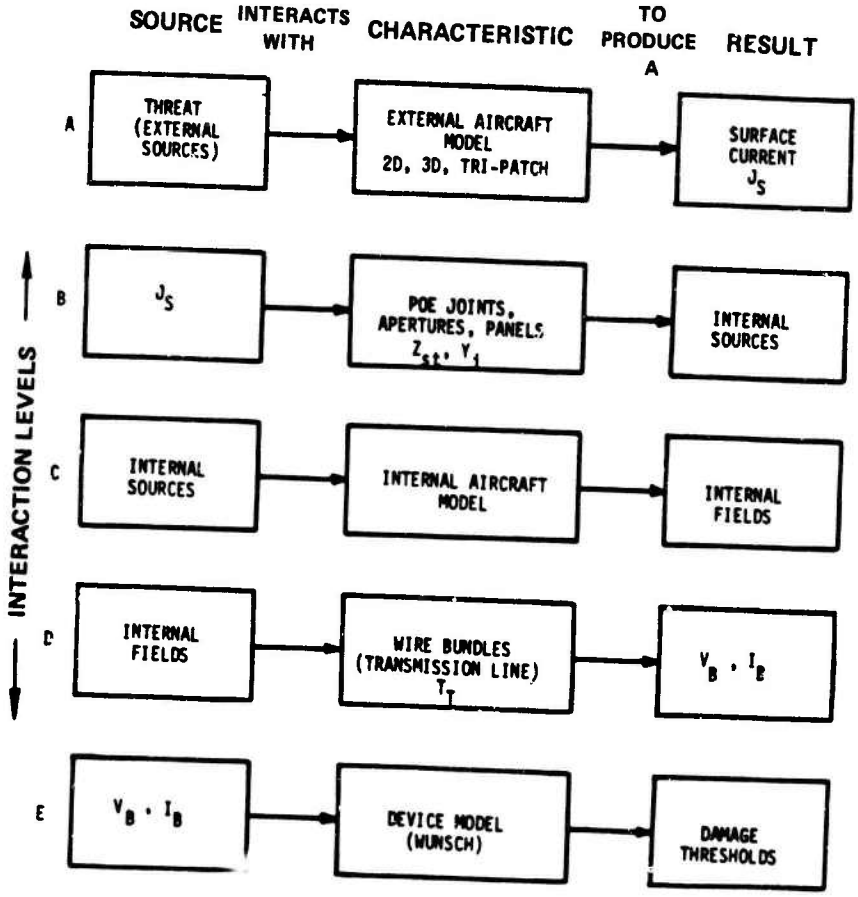

Fig. 1 - Interaction Partition Table

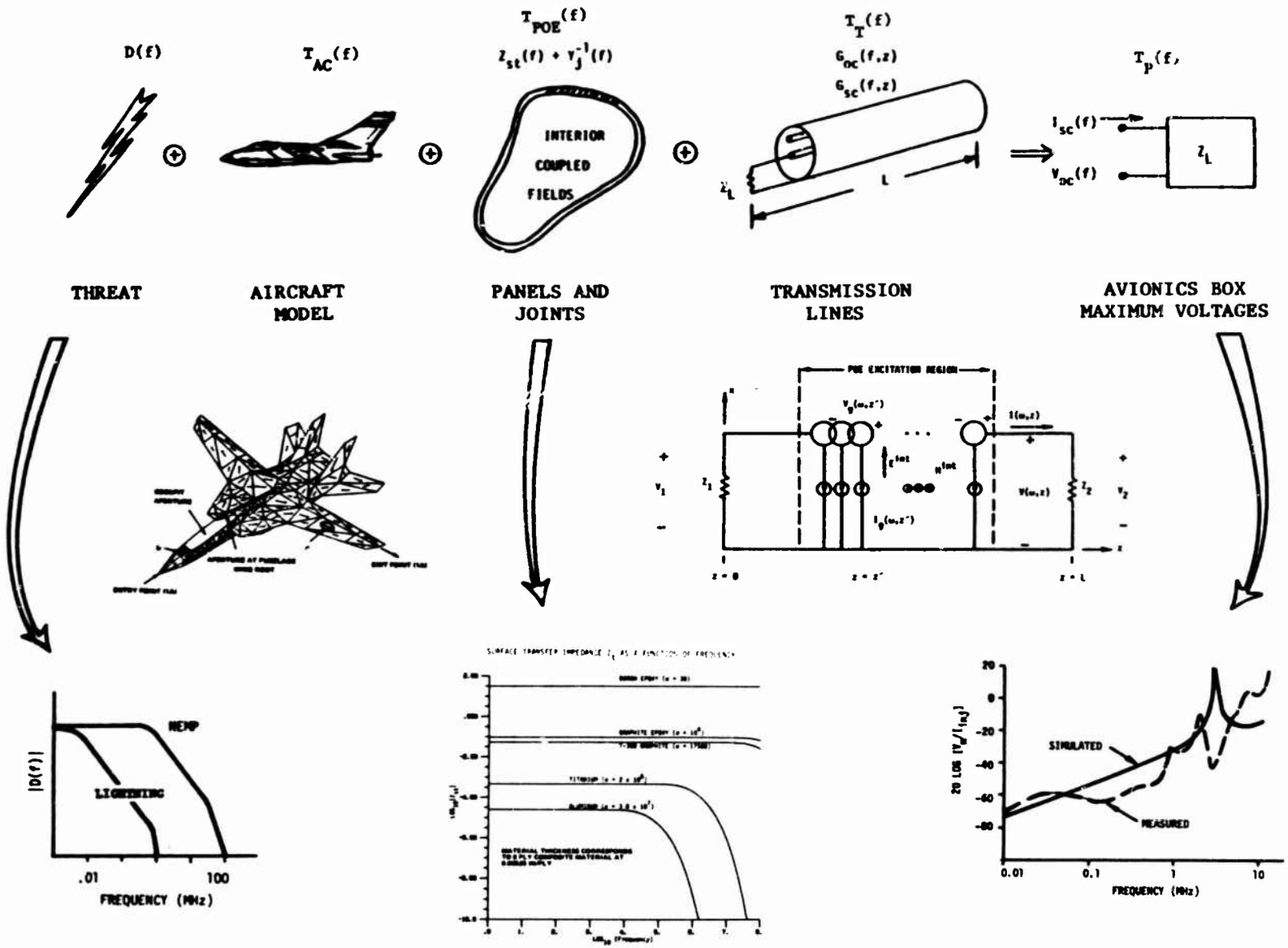

Fig. 2 - Frequency Domain Linear Cascaded Coupling Model

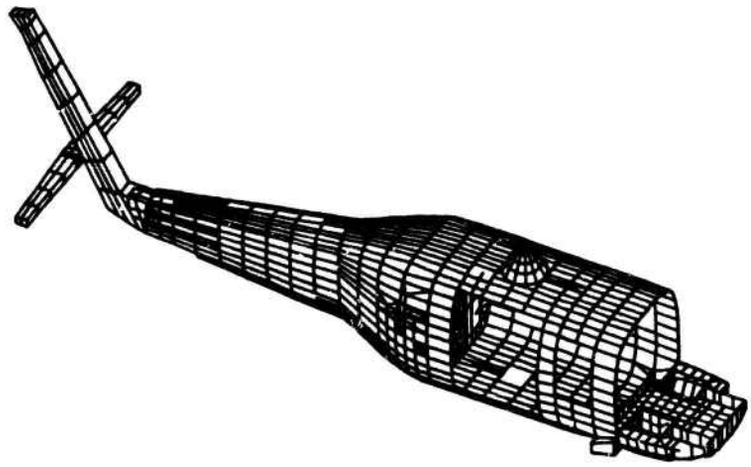

Fig. 3 - NASTRAN External Skin Data Base for Black Hawk Helicopter

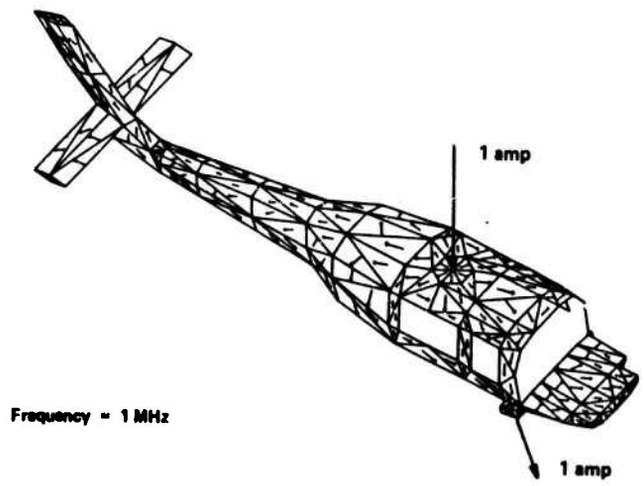

Fig. 4 - Top Oblique View of Black Hawk Showing Surface Currents $\mathrm{Re}\{\underline{J}_S\}$ for Main Rotor-to-Landing Gear Direct Strike Injection Current of 1 amp at Frequency of 1 MHz

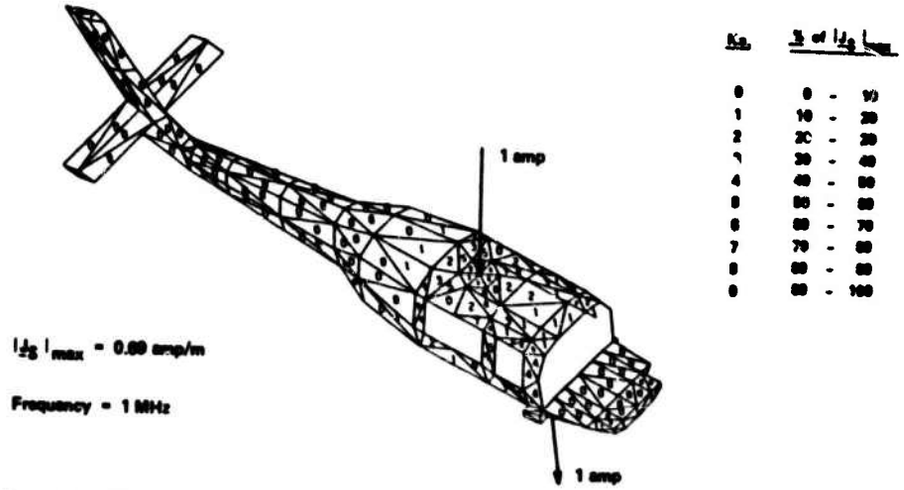

Fig. 5 - Top Oblique View of Black Hawk Showing Magnitudes of Current Vectors in Fig. 4 Scaled Relative to $|\underline{J}_S|_{max}$

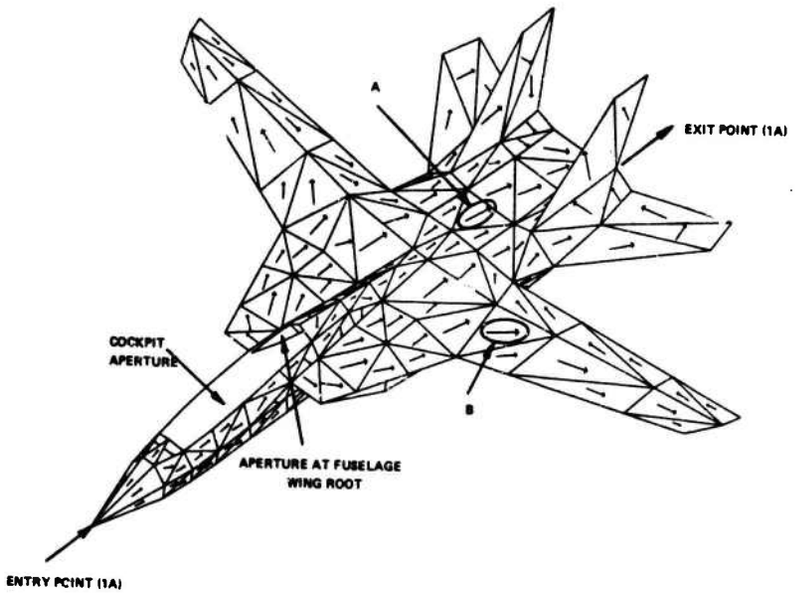

Fig. 6 - Top Oblique View of F-14 Showing Surface Currents $\mathrm{Re}\{\underline{J}^b\}$ for Nose-to-Tail Injection Current of 1 amp at Frequency of 1 MHz

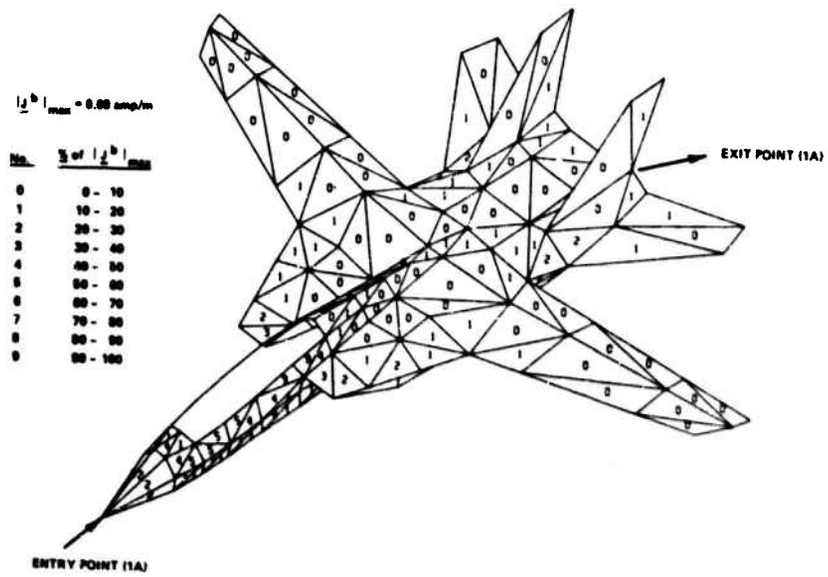

Fig. 7 - Illustration Showing Magnitudes of Current Vectors in Fig. 6 Scaled Relative to $|J^b|_{max}$

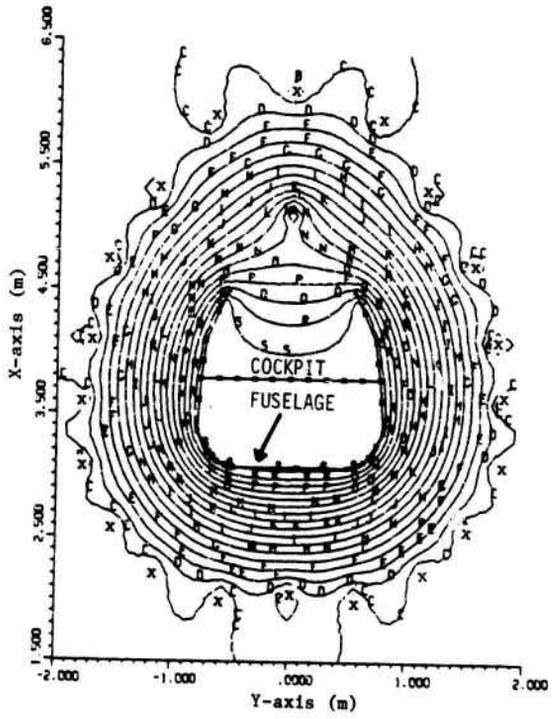

Equipotential lines at cross section of F-14 fuselage station 320 inside aircraft test fixture. The fuselage carries the injected current, which is returned to the generator by return conductors. This is used to estimate field levels inside large apertures and the total inductance of test fixtures.

x's indicate aircraft test fixture return conductors

ϕ_f = 83.39V (potential of fuselage)

ϕ_r = -16.61V (potential of return conductor

A ≡ -10V
.
.
.
S ≡ 80V

5V Intervals

Fig. 8 - Field Lines Inside F-14 Cockpit for Nose-Tail Strike

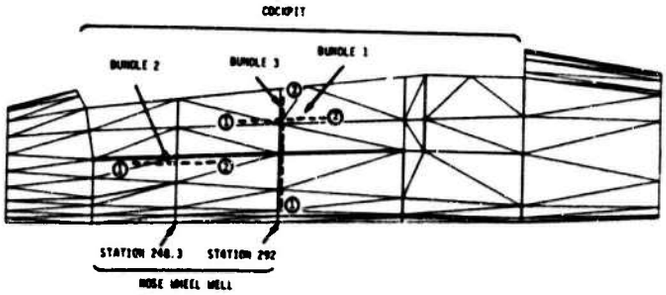

Example of transmission line model applied to F-14 wire bundle coupling in large aperture region. Distributed POE fields are computed by two-dimensional field penetration results.

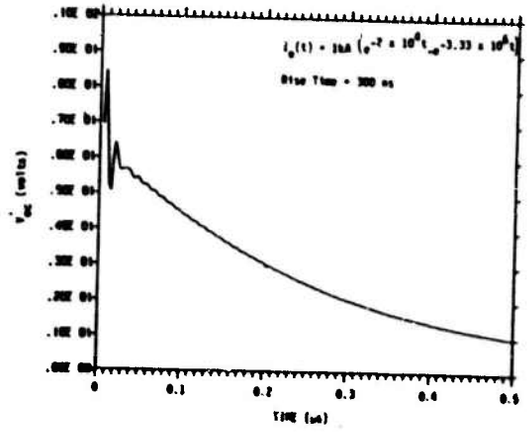

Open-circuit voltage at terminal 1 of Bundle 2 when Terminal 2 is terminated in 50Ω.

Fig. 9 - Generic Cable Bundle Results for F-14